Chemogenetic activation of adrenocortical Gq signaling causes hyperaldosteronism and disrupts functional zonation

Matthew J. Taylor,[1] Matthew R. Ullenbruch,[1] Emily C. Frucci,[1] Juilee Rege,[1] Mark S. Ansorge,[2] Celso E. Gomez-Sanchez,[3] Salma Begum,[4] Edward Laufer,[5] David T. Breault,[6] and William E. Rainey[1,7]

[1]Department of Molecular and Integrative Physiology, University of Michigan, Ann Arbor, Michigan, USA. [2]The Sackler Institute for Developmental Psychobiology, Columbia University, New York, New York, USA. [3]Endocrine Section, G.V. (Sonny) Montgomery VA Medical Center and the Department of Pharmacology and Toxicology, University of Mississippi Medical Center, Jackson, Mississippi, USA. [4]Department of Obstetrics, Gynecology and Women's Health, Rutgers, The State University of New Jersey, Newark, New Jersey, USA. [5]Department of Human Genetics, University of Utah, Salt Lake City, Utah, USA. [6]Department of Pediatrics, Division of Endocrinology, Boston Children's Hospital, Harvard Medical School, Boston, Massachusetts, USA. [7]Division of Metabolism, Endocrinology, and Diabetes, Department of Internal Medicine, University of Michigan, Ann Arbor, Michigan, USA.

The mineralocorticoid aldosterone is produced in the adrenal zona glomerulosa (ZG) under the control of the renin–angiotensin II (AngII) system. Primary aldosteronism (PA) results from renin-independent production of aldosterone and is a common cause of hypertension. PA is caused by dysregulated localization of the enzyme aldosterone synthase (Cyp11b2), which is normally restricted to the ZG. *Cyp11b2* transcription and aldosterone production are predominantly regulated by AngII activation of the Gq signaling pathway. Here, we report the generation of transgenic mice with Gq-coupled designer receptors exclusively activated by designer drugs (DREADDs) specifically in the adrenal cortex. We show that adrenal-wide ligand activation of Gq DREADD receptors triggered disorganization of adrenal functional zonation, with induction of Cyp11b2 in glucocorticoid-producing zona fasciculata cells. This result was consistent with increased renin-independent aldosterone production and hypertension. All parameters were reversible following termination of DREADD-mediated Gq signaling. These findings demonstrate that Gq signaling is sufficient for adrenocortical aldosterone production and implicate this pathway in the determination of zone-specific steroid production within the adrenal cortex. This transgenic mouse also provides an inducible and reversible model of hyperaldosteronism to investigate PA therapeutics and the mechanisms leading to the damaging effects of aldosterone on the cardiovascular system.

Introduction

The adrenal glands synthesize and secrete steroid hormones that play critical roles in the regulation of electrolyte balance, blood pressure, carbohydrate metabolism, and responses to stress. To accomplish these functions, the adrenal cortex is organized into functionally and histologically distinct zones. The outermost zona glomerulosa (ZG) is responsible for maintaining sodium and potassium balance through secretion of mineralocorticoids, predominantly aldosterone. Aldosterone synthesis and secretion are tightly controlled by the renin-angiotensin-aldosterone system (RAAS). The zona fasciculata (ZF) is controlled by adrenocorticotropic hormone (ACTH). ACTH regulates the production of glucocorticoids, primarily corticosterone and/or cortisol, to mediate stress responses. This functional zonation is maintained through differential expression of the enzymes required for mineralocorticoid versus glucocorticoid production. Murine lineage–tracing models have detailed the adrenal cell renewal process, which involves centripetal migration of steroidogenic cells and transdifferentiation of ZG cells into ZF cells. During development, this process initiates with the differentiation of subcapsular stem and progenitor cells into aldosterone-producing ZG cells. These cells are then displaced inward to the medullary border, where they undergo apoptosis, changing their zone-specific steroidogenic enzyme expression pattern throughout the process (1–9). A recent lineage-tracing study revealed that the outer ZG cells repopulate nearly the entire adrenal cortex within 3 months (1). The precise factors and mechanisms that regulate adrenocortical centripetal migration and the phenotypic switch from ZG to ZF cells remain unknown.

Physiologic regulation of aldosterone production involves the binding of angiotensin II (AngII) to its receptor angiotensin II receptor type 1 (AT_1R), resulting in activation of the Gq protein family. Gq signaling through phospholipase C increases cytosolic calcium, which then activates calcium/calmodulin-dependent kinases (CaMKs) (10–17). CaMKs initiate the activity of transcription factors that are critical for the transcription of aldosterone synthase (*Cyp11b2*) (18). Because of the ZG-specific localization of AT_1R and Cyp11b2 within the adrenal gland, aldosterone production is limited to adrenal ZG cells (19).

Conflict of interest: The authors have declared that no conflict of interest exists.

Submitted: February 26, 2019; **Accepted:** September 18, 2019;
Published: November 18, 2019.
Reference information: *J Clin Invest*. 2020;130(1):83–93.
https://doi.org/10.1172/JCI127429.

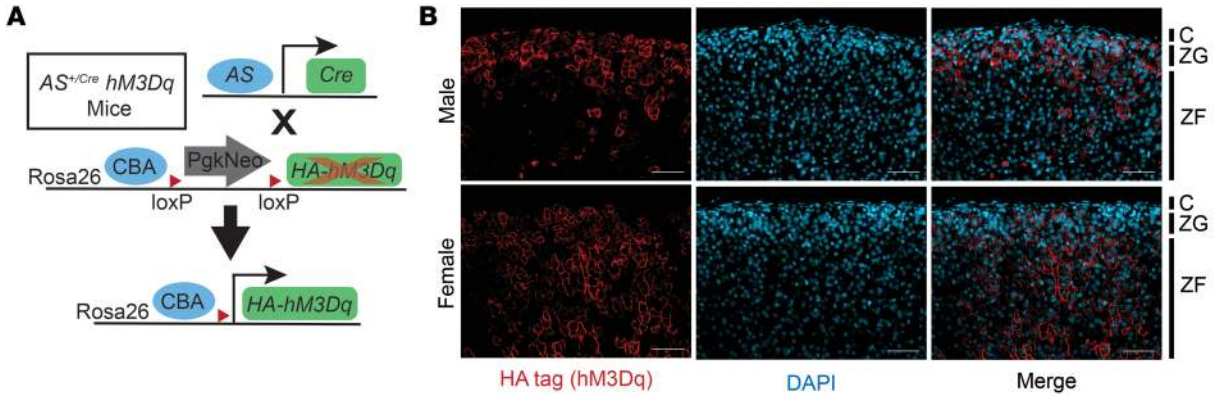

Figure 1. Adrenocortical-specific expression of hM3Dq driven by *AS*-Cre. (**A**) Schema of *AS*$^{+/Cre}$ *hM3Dq* mouse crossbreeding. *AS*-Cre mice were bred to be heterozygous for the Cre allele (*AS*$^{+/Cre}$) and crossed with the *hM3Dq* mouse line. Mice were bred on a homozygous *hM3Dq* background. Cre recombination resulted in an excision of the upstream Pgk-neomycin cassette (PgkNeo) at the loxP sites, allowing transcription of *hM3Dq* in Cre-positive cells. CBA, chicken β-actin promoter. (**B**) Immunofluorescence labeling of hM3Dq. The *hM3Dq* transgene has an HA tag, allowing for detection of the receptor via HA tag immunofluorescence. Adrenal glands from 20-week-old mice are shown. DAPI (blue) marks the nuclei. C, capsule. Scale bars: 50 μm.

Disruption of zone-specific expression of steroidogenic enzymes is one of the characteristics of diseases of steroid imbalance. One such disease is primary aldosteronism (PA), which is the most prevalent cause of secondary hypertension, affecting 5%–10% of patients with hypertension and 20% of those with resistant hypertension (20–26). Production of aldosterone that is independent of circulating renin causes inappropriate renal sodium retention and, consequently, high blood pressure. Patients with PA are therefore susceptible to severe cardiovascular risks and complications (27–31). In addition to causing hypertension, inappropriate aldosterone enhances deleterious effects on the cardiovascular system, including cardiac hypertrophy and fibrosis (32–35). Despite the high prevalence of PA and its associated mortality, animal models for this disease are limited (36).

Designer receptors exclusively activated by designer drugs (DREADDs) are modified GPCRs that bind synthetic ligands (37). This transgenic technology allows for chemogenetic activation of G protein signaling pathways. DREADD technology was originally applied to research in the neuroscience field (38) but has now been used in several tissues (39–44), including within an endocrine pancreatic β cells (45, 46). Here, we used a modified human M3 muscarinic receptor that couples to Gq (hM3Dq) and is activated by the ligand clozapine *N*-oxide (CNO) (38, 46–48). We developed transgenic mice with pan-adrenocortical expression of hM3Dq receptors. Activation of adrenal Gq signaling promoted ectopic localization of Cyp11b2 in the ZF. Mice exhibited a PA phenotype with renin-independent aldosterone production and hypertension. Furthermore, beyond triggering hyperaldosteronism, the presence of Gq signaling may contribute to maintenance of the ZG cellular phenotype as well.

Results

Generation of AS$^{+/Cre}$ *hM3Dq mice*. *hM3Dq* mice have a transgene that encodes the hM3Dq DREADD (47). The *hM3Dq* transgene is transcribed exclusively in the presence of Cre recombinase and contains an HA tag sequence (47). Expression of *hM3Dq* was driven specifically to the adrenal cortex by crossing *hM3Dq* mice with aldosterone synthase Cre (*AS*-Cre) mice (Figure 1A). *AS*-Cre mice have Cre recombinase inserted into the *Cyp11b2* locus (1). Mice were bred to be heterozygous for *AS*-Cre (*AS*$^{+/Cre}$ *hM3Dq*), which allowed them to maintain *Cyp11b2* expression (1). The presence and localization of hM3Dq were confirmed by HA tag immunofluorescence (IF) staining. Adrenal *Cyp11b2* expression arises after birth, therefore, low levels of adrenal hM3Dq were present in these mice early in life, at 3 weeks of age (Supplemental Figure 2; supplemental material available online with this article; https://doi.org/10.1172/JCI127429DS1). Centripetal migration of Cre-recombined cells led to adrenocortical hM3Dq abundance that increased throughout life (Supplemental Figure 2). The majority of cortical cells in these mice contained hM3Dq by 20 weeks of age, with no presence of the receptor in the medulla (Figure 1). Given this caveat, we used *AS*$^{+/Cre}$ *hM3Dq* mice that were 18–22 weeks of age. The expression of hM3Dq in the ZG and ZF allows for the activation of Gq signaling in both zones upon treatment with CNO (Supplemental Figure 1). In mice that lacked Cre and were WT for AS (*AS*$^{+/+}$ *hM3Dq* mice), we did not detect HA tag staining of hM3Dq (data not shown).

Cortical activation of Gq signaling results in hyperaldosteronism. Female *AS*$^{+/Cre}$ *hM3Dq* mice were treated with CNO or vehicle for 7 days (Figure 2A), and adrenal RNA was isolated and analyzed for transcripts encoding steroid-metabolizing enzymes (Figure 2B). CNO-treated female *AS*$^{+/Cre}$ *hM3Dq* mice had a significant 6.5-fold increase in *Cyp11b2* transcript levels above those of vehicle-treated mice, as assessed by quantitative real-time PCR (qPCR) (Figure 2C). This observation correlated with an increase in Cyp11b2 protein levels and 3.1-fold higher circulating aldosterone levels in CNO-treated females (Figure 2, D and E). Interestingly, zonation of Cyp11b2 was disordered, as we found Cyp11b2-positive cells in the ZF as well as in the ZG. Double-IF indicated that some ZF cells coexpressed Cyp11b1 and Cyp11b2, with a smaller subset exclusively containing Cyp11b2 (Figure 2D). The increase in aldosterone levels was variable, with some CNO-treated mice producing more than 1000 pg/mL aldosterone, whereas others showed more moderate increases (Figure 2E). The final steroid precursor for the synthesis of aldosterone 18-hydroxycorticosterone (18OHB) was also significantly increased (2.6-fold) following CNO treatment (Supplemental Table 1). We found that *Ren1* mRNA, the mouse transcript that encodes renin in

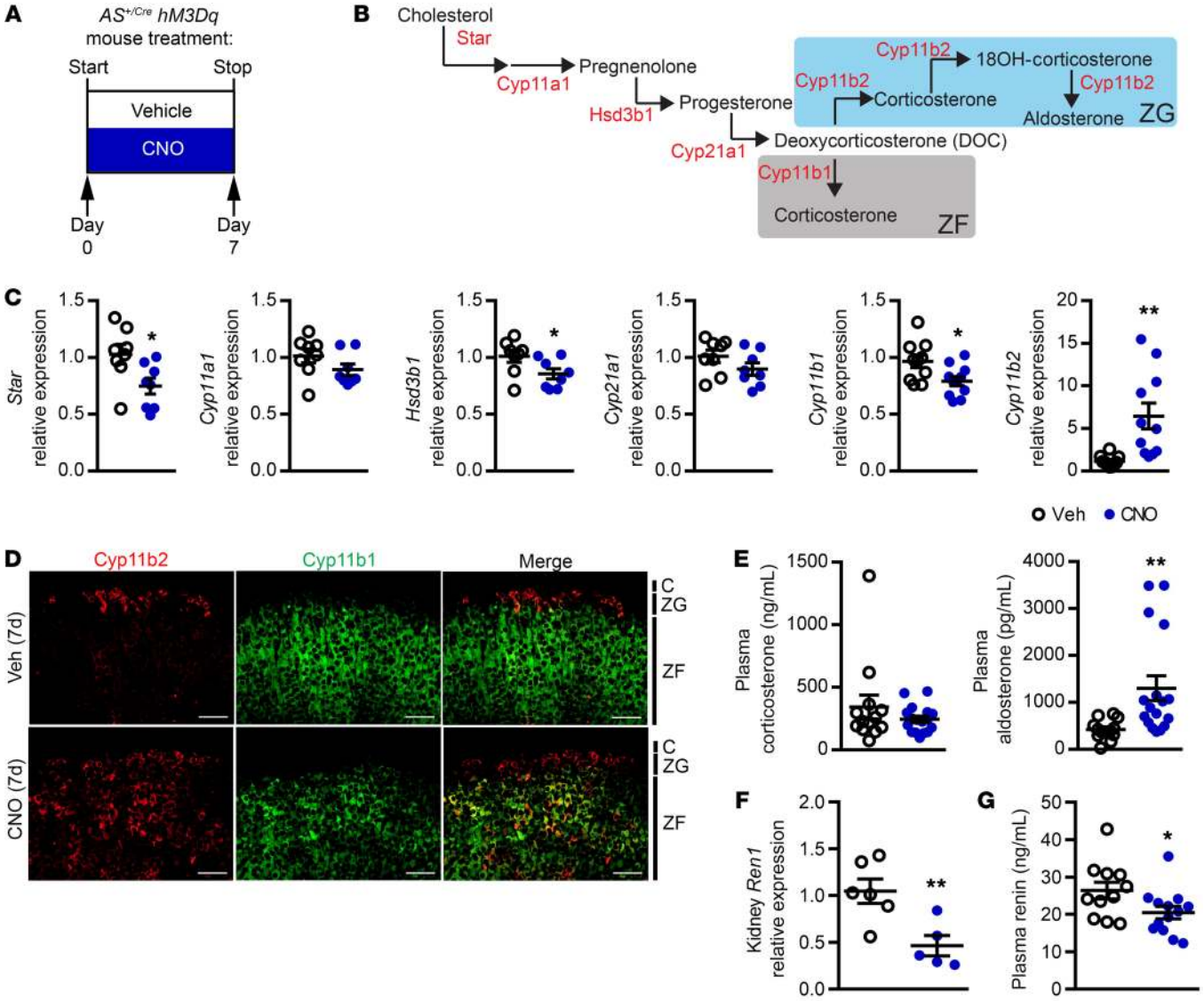

Figure 2. CNO activation of adrenal hM3Dq upregulates Cyp11b2 expression and aldosterone production. (**A**) Experimental protocol. *AS*$^{+/Cre}$ *hM3Dq* female 18- to 20-week-old mice were treated with CNO (50 μg/mL) or vehicle in their drinking water (ad libitum) for 7 days prior to sacrifice. (**B**) Mouse adrenal steroidogenic pathway. Star transports cholesterol to the inner mitochondrial membrane, where it is converted to pregnenolone prior to downstream conversion to either glucocorticoids (ZF) or mineralocorticoids (ZG) by steroidogenic enzymes. (**C**) qPCR analysis of steroidogenic enzyme mRNA in whole adrenal tissue. $n = 8$ for both groups for steroidogenic enzymes; $n = 10$ for *Cyp11b1* and *Cyp11b2* (vehicle treatment); $n = 11$ for *Cyp11b1* and *Cyp11b2* (CNO treatment). (**D**) Immunofluorescence staining for Cyp11b2 and Cyp11b1. Scale bars: 50 μm. (**E**) Steroid levels were measured by LC-MS/MS. $n = 13$ for vehicle treatment; $n = 17$ for CNO treatment. (**F**) qPCR analysis of kidney *Ren1*. $n = 6$ for vehicle treatment; $n = 5$ for CNO treatment. (**G**) Plasma renin concentrations. $n = 11$ for vehicle treatment; $n = 13$ for CNO treatment. Data in the dot plots represent the mean ± SEM. $^*P < 0.05$ and $^{**}P < 0.01$, by unpaired, 2-tailed Student's *t* test. Veh, vehicle.

the juxtaglomerular renal cells, was significantly decreased in the kidneys of CNO-treated female mice (Figure 2F), as were plasma renin concentrations (Figure 2G), suggesting a suppression of the RAAS. This confirmed that the hM3Dq-induced aldosterone production was renin independent, as seen in PA. Of the genes encoding adrenal steroidogenic enzymes, *Cyp11b2* was the only upregulated gene in the CNO-treated mice (Figure 2C). Furthermore, *Star, Hsd3b1,* and *Cyp11b1* all had small but significant decreases in expression, with downward trends also observed for transcripts encoding the other steroidogenic enzymes (Figure 2C). The slight decrease in transcript levels for these enzymes may be related to normalization of gene expression relative to *Ppia*, which is expressed in both the cortex and medulla. Normalization to a transcript expressed only in the cortex, steroidogenic factor 1 (*Sf1*), eliminated this effect in these transcripts, except for *Star*, which was still decreased, but to a lesser degree than that seen with *Ppia* normalization (data not shown). These data demonstrate that the increase in aldosterone secretion in CNO-treated mice was a direct effect of increased Cyp11b2 transcript and protein levels rather than of targeted increases in other enzymatic steps in steroidogenesis. Despite the slight decrease in *Cyp11b1* transcription, we did not detect a significant decrease in plasma corticosterone levels (Figure 2E). It is worth noting that 7 days of CNO treatment did not alter aldosterone or *Cyp11b2* transcript levels in the *AS*$^{+/+}$ *hM3Dq* littermate control mice (Supplemental Figure 3).

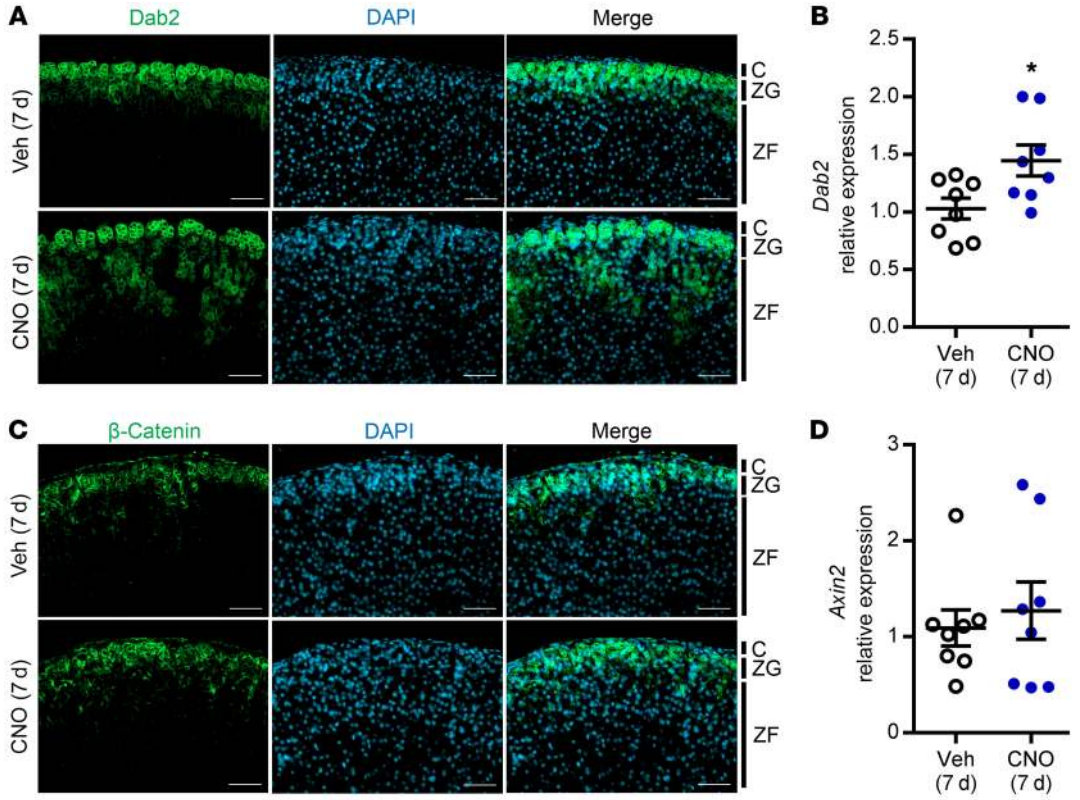

Figure 3. *AS*$^{+/Cre}$ *hM3Dq* mice have increased expression of the ZG marker Dab2, with no changes in the ZG-specific Wnt pathway. (**A**) Immunofluorescence staining for the ZG-specific Dab2 protein (green). (**B**) qPCR analysis for whole adrenal *Dab2* mRNA. (**C**) Immunofluorescence staining for active β-catenin (green). (**D**) qPCR analysis for whole adrenal mRNA expression of the Wnt pathway target gene *Axin2*. $n = 8$ for both CNO- and vehicle-treated groups in **B** and **D**. DAPI (blue) stained the nuclei in **A** and **C**. Scale bars: 50 μm. Data in the dot plots represent the mean ± SEM. $^*P < 0.05$, by unpaired, 2-tailed Student's *t* test.

Female *AS*$^{+/Cre}$ *hM3Dq* mice did not have a significant difference in body weight following 7 days of CNO treatment (Supplemental Figure 4A). Interestingly, we observed a minor but significant decrease in adrenal gland size relative to body weight in CNO-treated female mice in the left adrenal gland and a trend toward a decrease in the right adrenal gland (Supplemental Figure 4C). Nevertheless, we observed no obvious changes to adrenal gland morphology, as assessed by H&E staining after 7 days of CNO treatment (Supplemental Figure 4B).

Also, after 7 days of CNO treatment, male *AS*$^{+/Cre}$ *hM3Dq* mice responded with significantly upregulated plasma aldosterone production (1.8-fold compared with control mice) (Supplemental Figure 5C). However, we detected no change in *Cyp11b2* mRNA levels in these mice (Supplemental Figure 5A). Cyp11b2 protein was localized to the ZG, with low levels detected in the ZF (Supplemental Figure 5B). The increase in aldosterone did not inhibit renin production in male mice, as we observed no difference in kidney *Ren1* transcript levels between groups (Supplemental Figure 5D). This sexually dimorphic response could partly be explained by the unequal hM3Dq expression at 20 weeks of age in males and females (Figure 1B). Notably, previous mouse models that have used the *AS*-Cre mouse line to drive adrenal cortex–specific Cre expression have exhibited similar sex differences (49, 50).

Gq signaling contributes to the ZG cell phenotype. We also examined the expression of disabled homolog 2 (Dab2), a ZG-specific protein that participates in aldosterone production and is regulated by AngII (51). Following 7 days of CNO treatment, Dab2 was no longer restricted to the ZG in female mice, as several ZF cells were also positive for Dab2 (Figure 3A). This coincided with a 1.5-fold increase in *Dab2* transcript levels in the adrenal glands of female *AS*$^{+/Cre}$ *hM3Dq* mice treated with CNO (Figure 3B).

Wnt/β-catenin signaling plays an important role in adrenal development, growth, and cell replenishment and is preferentially active in the ZG compared with other cortical zones (52–58). Therefore, we determined whether chemogenetic Gq signaling would be sufficient to upregulate Wnt/β-catenin signaling. qPCR analysis for the canonical Wnt pathway target gene *Axin2* revealed no change between vehicle and CNO-treated groups, suggesting that the pathway is not activated in response to Gq signaling (Figure 3D). Consistent with this, IF showed that β-catenin localization was limited to the ZG in both control and CNO-treated female mice, with only minor expression in the outer ZF cells (Figure 3C). This suggests that the Cyp11b2-positive ZF cells did not undergo a complete phenotypic switch to ZG cells. It also indicates that aldosterone production per se is not reliant on Wnt/β-catenin signaling, as expression of ZF Cyp11b2 is able to turn on following activation of Gq signaling.

hM3Dq-induced aldosterone production bypasses high-sodium diet–induced suppression of the RAAS. High-sodium (HS) diets inactivate adrenal aldosterone synthesis through suppression of renin under normal physiological conditions (59). This was apparent in

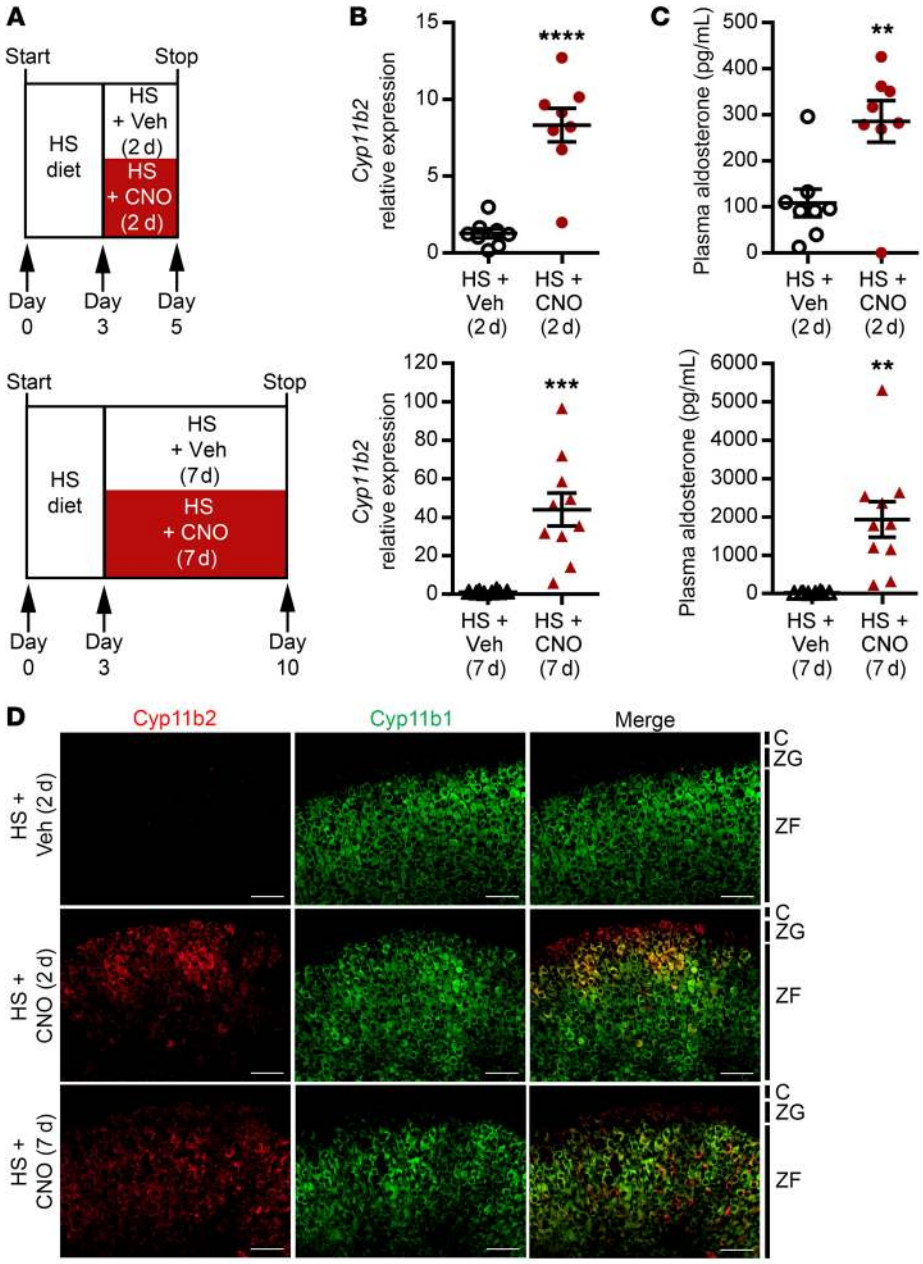

Figure 4. *AS*$^{+/Cre}$ *hM3Dq* mice activate Cyp11b2 and aldosterone production in the presence of a HS diet. (**A**) Female 20- to 22-week-old *AS*$^{+/Cre}$ *hM3Dq* mice were fed a HS diet for 3 days. One group then received HS plus CNO or HS plus vehicle for 2 days, and the other group received HS plus CNO or HS plus vehicle for 7 days prior to sacrifice. (**B**) qPCR analysis for whole adrenal *Cyp11b2* mRNA. (**C**) LC-MS/MS analysis of plasma aldosterone concentration. (**D**) Immunofluorescence staining of Cyp11b2 (red) and Cyp11b1 (green). Scale bars: 50 μm. For steroid and qPCR analysis, $n = 8$ for all groups, except for the 7-day HS plus CNO treatment group, where $n = 10$. Data in the dot plots represent the mean ± SEM. $^{**}P < 0.01$, $^{***}P < 0.001$, and $^{****}P < 0.001$, by unpaired, 2-tailed Student's *t* test.

AS$^{+/Cre}$ *hM3Dq* mice fed a HS diet for 3 days prior to CNO treatment. To determine whether CNO treatment could override RAAS suppression, mice were split into 2 groups: (a) HS diet plus 2 days of CNO treatment (2-day HS plus CNO) and (b) HS diet plus 7 days of CNO treatment (7-day HS plus CNO) (Figure 4A). Alongside these groups, we used littermate mice treated with a HS diet plus vehicle (HS plus vehicle) as controls. The 2 time points allowed us to examine the temporal regulation of aldosterone synthesis by the hM3Dq system. In female mice administered HS plus CNO for 2 days, we found that plasma aldosterone significantly increased by 2.6-fold and that *Cyp11b2* mRNA levels increased by 8.3-fold above the levels seen in the control mice treated with HS plus vehicle (Figure 4, B and C). Assessment of IF staining revealed Cyp11b2 protein expression in the ZG and the ZF at variable levels (Figure 4D). On day 2 of treatment, we found that ZF Cyp11b2 was almost exclusively coexpressed with Cyp11b1 in the majority of mice. In comparison, mice that were treated with HS plus CNO for 7 days showed a robust, 105-fold increase in aldosterone production through an upregulation of *Cyp11b2* transcript levels by 44-fold relative to the control mice treated with HS plus vehicle (Figure 4, B and C). The levels of aldosterone in these mice treated for 7 days with HS plus CNO averaged 1949 pg/mL, a remarkable increase from the 285 pg/mL average of the mice treated for 2 days with HS plus CNO. 18OHB concentrations also increased significantly in both the 2-day (1.8-fold) and 7-day (33-fold) treatment cohorts (Supplemental Table 1). No significant changes were observed in 11DOC or corticosterone concentrations under these conditions (Supplemental Table 1). Moreover, the level and disorganization of Cyp11b2 protein localization were higher in the samples from mice treated for 7 days than in those from mice treated for 2 days

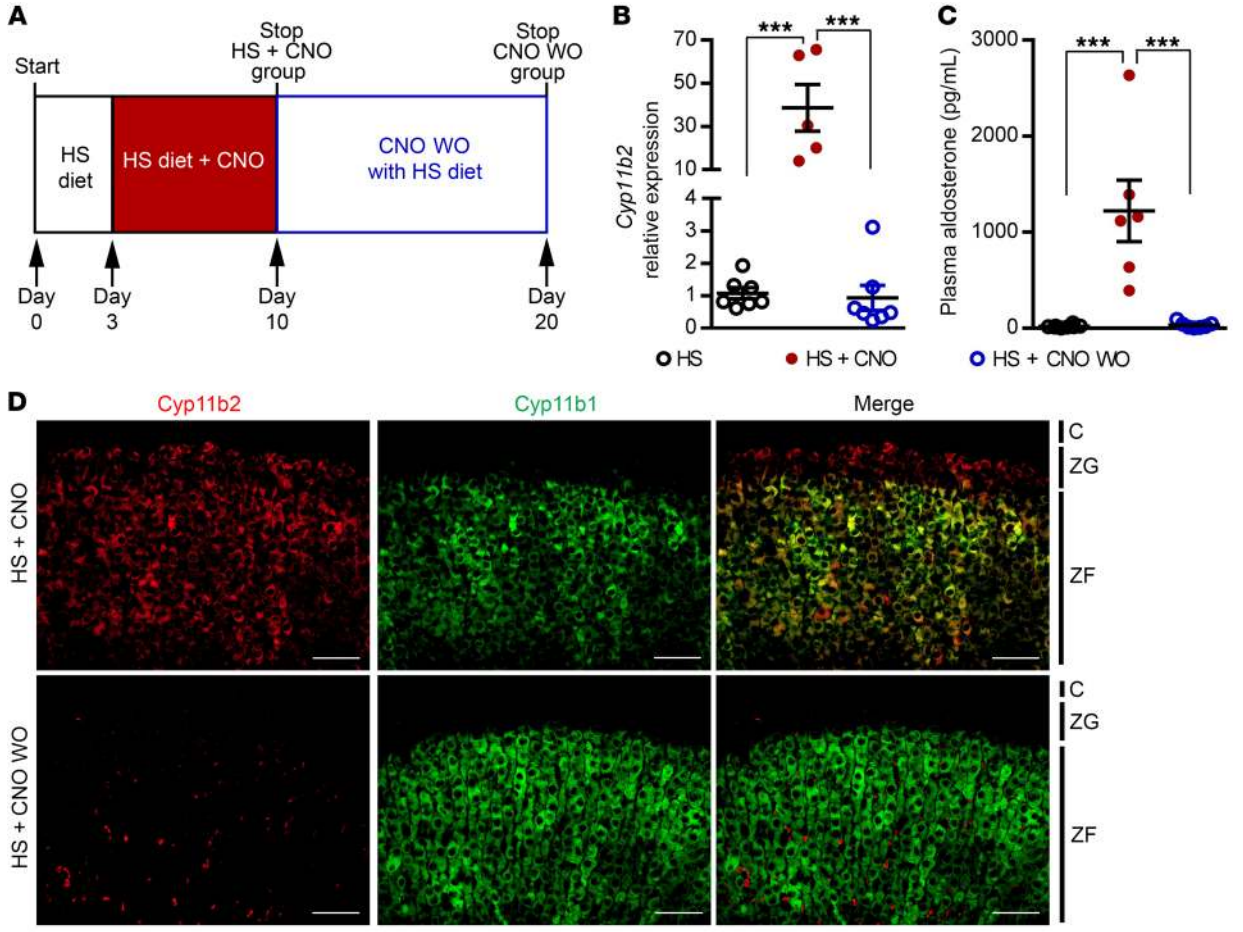

Figure 5. CNO washout causes reversal of the PA phenotype in *AS*$^{+/Cre}$ *hM3Dq* mice. (**A**) Experimental protocol. Female 20- to 22-week-old *AS*$^{+/Cre}$ *hM3Dq* mice were treated with a HS diet for 3 days. All mice were then administered HS plus CNO for 7 days. One group was sacrificed on day 7 (HS + CNO), whereas the other group underwent a washout (WO) protocol for an additional 10 days with a HS diet but without CNO (HS + CNO WO). (**B**) qPCR analysis of whole adrenal *Cyp11b2* mRNA. For qPCR analysis, HS plus vehicle treatment, $n = 7$; for HS plus CNO treatment, $n = 5$; and for HS plus CNO washout, $n = 7$. (**C**) LC-MS/MS measurement of plasma aldosterone levels. For steroids, HS plus vehicle treatment, $n = 8$; for HS plus CNO treatment, $n = 6$; and for HS plus CNO washout, $n = 7$. (**D**) Immunofluorescence staining for Cyp11b2 (red) and Cyp11b1 (green). Scale bars: 50 μm. For **B** and **C**, the previously described controls treated with HS plus vehicle (Figure 4) were used as a comparison for the HS plus CNO and HS plus CNO washout groups. Data in the dot plots represent the mean ± SEM. ***$P < 0.001$, by 1-way ANOVA with Bonferroni's correction.

(Figure 4D). These mice also had a subset of ZF cells with exclusive expression of Cyp11b2 after 7 days of HS plus CNO treatment (Figure 4D). These observations validate the ability of CNO to elevate aldosterone secretion independently of renin, even at an early time point. In addition, these data suggest that prolonged activation of ZF Gq signaling can promote the development of an aldosterone-producing cellular phenotype.

We also assessed male *AS*$^{+/Cre}$ *hM3Dq* mice in this cohort. At the 2-day time point, we found that male mice treated with HS plus CNO had a 3.8-fold upregulation in circulating aldosterone, with an average of 289 pg/mL (Supplemental Figure 5F). In addition, adrenal *Cyp11b2* transcript levels increased by 9.7-fold (Supplemental Figure 5E). The 2-day treatment response in male mice was similar to that seen in females, but in the treatment group that received 7-day HS plus CNO, the response of males diverged from that of females, with male mice showing lower levels of circulating aldosterone (482 pg/mL average) and adrenal *Cyp11b2* (6.5-fold compared with controls) (Supplemental Figure 5, E and F).

Washout of CNO normalizes the PA phenotype in AS$^{+/Cre}$ *hM3Dq mice*. To address whether the PA phenotype observed in the *AS*$^{+/Cre}$ *hM3Dq* was reversible, we designed a CNO washout experiment. To suppress physiological RAAS activation, all mice were fed a HS diet for a 3-day period and then given HS plus CNO for 7 days. After this treatment period, 1 group of mice was sacrificed, whereas another group of littermates was maintained on a HS diet without CNO treatment (Figure 5A). For analysis of mRNA and steroid data, we compared both groups with the previously described group that were treated for 7 days with HS plus vehicle (Figure 4). Mice treated with HS plus CNO had robust elevations of both Cyp11b2 and aldosterone, with the same level of zonal dysregulation in Cyp11b2 localization as described above (Figure 5, B–D). Strikingly, upon CNO removal, 10 days was sufficient to reverse the phenotype for all parameters back to baseline levels (Figure 5, B–D). CNO washout also led to normalization of adrenal *Cyp11b2* mRNA expression and plasma aldosterone levels in mice maintained on a normal sodium (NS) diet (data not shown).

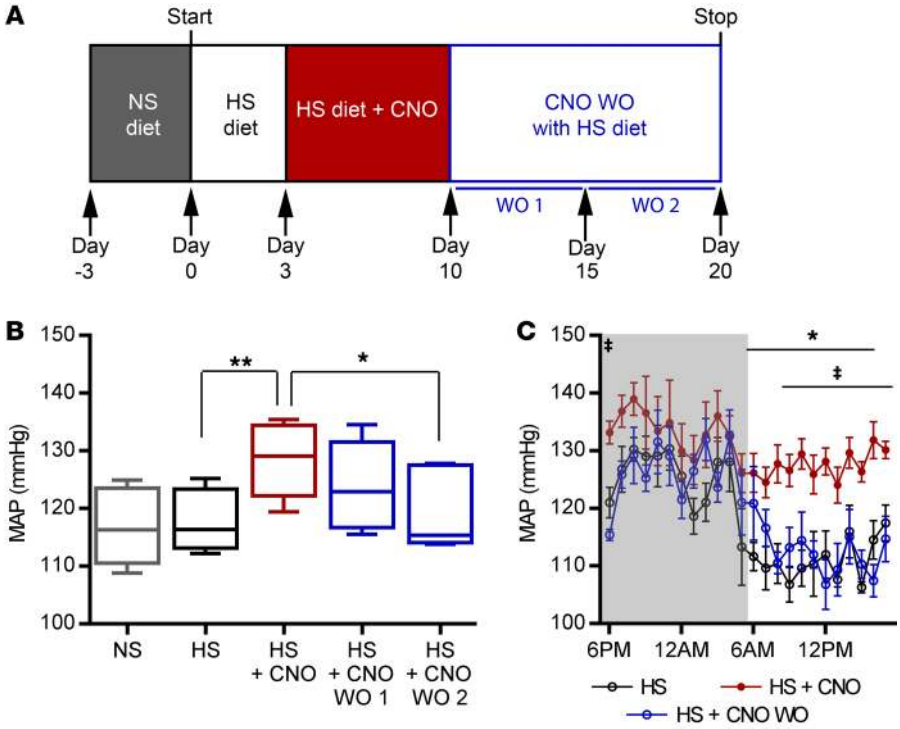

Figure 6. A HS diet plus CNO increases blood pressure in *AS*$^{+/Cre}$ *hM3Dq* mice. (**A**) Experimental protocol. Female 20-week-old *AS*$^{+/Cre}$ *hM3Dq* mice (n = 5) were implanted with a radiotelemetric device and given 2 weeks for recovery. The final 4 days prior to treatment were analyzed as the baseline. Mice were then fed a HS diet for 3 days, HS plus CNO for 7 days, and HS alone (CNO washout) for 10 days. MAP was continuously recorded throughout the experiment. (**B**) Average MAP in the NS diet, HS diet, HS plus CNO, and HS plus CNO washout treatment periods (separated into 2 consecutive 5-day periods). Data in **B** represent the interquartile range with the median (box) and the minimum and maximum (whiskers). (**C**) Hourly MAP overlaid for the same mice using the final 24 hours of a HS diet alone (black circles), the second day of HS plus CNO treatment (day 4 in **A**, red circles), and the seventh day of HS plus CNO washout. The gray box signifies the dark (active) period. The second day of HS plus CNO treatment was chosen to allow orally given CNO to raise aldosterone levels. Data in **C** represent the mean ± SEM for the mice for each hour. (**B**) $^*P < 0.05$ and $^{**}P < 0.01$, by repeated-measures 1-way ANOVA with Bonferroni's correction. (**C**) $^*P < 0.05$, for the HS diet versus HS plus CNO; $^‡P < 0.05$, for HS plus CNO versus HS plus CNO washout; by repeated-measures 2-way ANOVA with Bonferroni's correction.

hM3Dq activation causes hypertension. To ascertain whether the adrenal and steroid phenotype in the *AS*$^{+/Cre}$ *hM3Dq* mice recapitulated the hypertension seen in PA, we evaluated the blood pressure in these mice. Radiotelemetric device implantation allowed for continuous monitoring of blood pressure in real time. After recovery from surgery, the female mice were given a HS diet for 3 days, followed by 7 days of HS plus CNO treatment (Figure 6A). A HS diet alone did not elevate the mean arterial pressure (MAP), whereas a HS diet combined with CNO increased blood pressure by an average of 11.2 mmHg compared with the HS diet alone across the full treatment period (Figure 6B). Treatment caused similar increases in both systolic and diastolic pressures (data not shown). Upon CNO removal, MAP gradually normalized to pre-CNO levels over a 10-day washout period with a continued HS diet. We also analyzed the changes in MAP within each hour across 24 hours, under each treatment condition. Interestingly, we found that hourly MAPs were mostly unchanged during the dark cycle (active period) in CNO-treated mice (Figure 6C). However, significant increases in MAP in the HS plus CNO treatment group versus the HS-alone group were observed at nearly every hour of the light cycle (inactive period) (Figure 6C). This finding suggests that the increase in MAP in female *AS*$^{+/Cre}$ *hM3Dq* mice is partly due to a disruption of the circadian rhythm of blood pressure. Additionally, in the HS plus CNO washout phase compared with the HS plus CNO treatment phase, we detected a significant decrease in MAP at most hours of the light cycle to near-baseline levels. We detected no differences between the HS phase and the HS plus CNO washout phase, illustrating a reversibility in the blood pressure phenotype. It is worth noting that under the same protocol, male mice also responded to HS plus CNO treatment with a significant increase in MAP, albeit a smaller increase than that seen in female mice (data not shown).

Discussion

The current study suggests that in *AS*$^{+/Cre}$ *hM3Dq* mice, activation of Gq signaling is sufficient to cause glucocorticoid-producing ZF cells to produce aldosterone. The ectopic expression of Cyp11b2 leads to renin-independent hyperaldosteronism, resulting in a significant increase in MAP. The disruption of functional zonation and aldosterone production were reversed upon removal of the activating ligand CNO. Taken together, our analysis of hM3Dq expression specifically in the adrenal cortex provides insights into adrenocortical cell plasticity and an inducible/reversible mouse model for the study of PA.

There are several features that define the adrenal ZG. These include the zone-specific expression of Cyp11b2 and the capacity to produce aldosterone. It is also the ZG that provides the cells needed to repopulate the adrenal cortex through centripetal migration. Activation of hM3Dq receptors partially reverted ZF cells to a ZG phenotype, particularly with regard to aldosterone production. This was illustrated by the ZF expression of Cyp11b2 and the elevated circulating aldosterone levels. We also detected expression of the ZG-specific protein Dab2 (51, 60) in some ZF cells following CNO treatment, as well as a significant increase ($P < 0.05$) in *Dab2* adrenal mRNA levels. These findings imply that it may be the ZF loss of AT_1R expression and, consequently, the loss of AngII-mediated Gq signaling that allow a ZG-to-ZF cell transition. However, it appears that Gq signaling alone is not sufficient for a complete ZF-to-ZG cell reversal. Our data suggest that activation of Gq signaling throughout the adrenal cortex does not alter the localization of Wnt/β-catenin signaling, which is primarily a ZG-restricted pathway. Wnt/β-catenin signaling has an important role in adrenal development and tissue homeosta-

sis (54). Within the ZG, most cells are positive for both β-catenin and Cyp11b2 (52), and it has been suggested that Wnt/β-catenin signaling can control aldosterone production (57, 61). Activating mutations in *CTNNB1*, the gene that encodes β-catenin, have also been described in a small subset of human aldosterone-producing adenomas (62–65). Therefore, although it is clear that the Wnt/β-catenin pathway is involved in ZG aldosterone production, these data demonstrate that it may not be essential for the Gq signaling steps downstream of AT_1R binding of AngII. This aligns with the previously reported role of β-catenin in stimulating AT_1R expression (57), a mechanism that is upstream of hM3Dq-induced Gq activation. It is also possible that Wnt/β-catenin signaling can activate aldosterone synthesis through a separate mechanism outside of regulating the potential for Gq signaling.

With the *AS*$^{+/Cre}$ *hM3Dq* mouse model, we created a tool that researchers can use to study PA, hypertension, and peripheral tissue damage caused by inappropriate aldosterone production. There are several previously described mouse models that exhibit a PA phenotype. A series of studies have linked constitutive inactivation of various potassium channels to hyperaldosteronism in vivo (66–73). The *task1*$^{-/-}$ mice are similar to *AS*$^{+/Cre}$ *hM3Dq* mice, in that they also exhibit ZF localization of Cyp11b2 without development of hyperplasia or adrenal nodules, and this phenotype is particularly evident in female mice (67). In this way, both models appear to involve a switch in cellular phenotype, specifically in ZF cells, that leads to overproduction of aldosterone. However, in *task1*$^{-/-}$ mice, the hyperaldosteronism state has been suggested to result from ACTH stimulation that induces Cyp11b2 in ZF cells (67). Thus, the *task1*$^{-/-}$ mouse is phenotypically similar to individuals with familial hyperaldosteronism type 1 (glucocorticoid-suppressible aldosteronism). Disruption of the circadian clock through *Cry1/Cry2* knockout also caused elevated plasma aldosterone and salt-sensitive high blood pressure (74). One study used a mutagenesis screen to link mutations to hyperaldosteronism phenotypes (75). Increases in aldosterone synthesis and salt-sensitive blood pressure were also accomplished through transgenic stabilization of the 3′-UTR of *Cyp11b2* or overexpression of the human *CYP11B2* gene (76, 77). Most recently, inactivation of an E3 ubiquitin ligase, Siah1, increased Cyp11b2 expression and aldosterone production (60).

It is also important to note that this is not the first mouse model of Gq signaling activation to mimic RAAS-related hypertension. A mouse model with a global gain-of-function mutation in *Agtr1a* (AT_{1A} receptor [$AT_{1A}R$]) mimicked low-renin hypertension, albeit with normal aldosterone levels but a high aldosterone-to-renin ratio (78). In vitro studies of this $AT_{1A}R$ mutation increased basal receptor activity, but not to the level seen following AngII treatment of WT or mutant receptor–expressing cells (79). Thus, it is likely that adrenal ZG $AT_{1A}R$ activity is increased, but the resulting suppression of renin limits the rise in circulating aldosterone levels. In contrast, CNO treatment of *AS*$^{+/Cre}$ *hM3Dq* mice allows aldosterone levels to rise to the pathologic range despite a suppression of renin.

Importantly, related to the *AS*$^{+/Cre}$ *hM3Dq* mouse model, there are clinical correlates for inappropriate activation of GPCRs in both adrenal Cushing's syndrome and PA (80). Aldosterone-producing tumors have been shown to ectopically express multiple receptors that can substitute for the normal function of AngII and cause aldosterone excess (81–84). The mechanisms that cause aberrant receptor expression in aldosterone-producing tumors remain unclear but may relate to the somatic gene mutations found in these tumors (84).

Although previous findings have advanced the field, the aforementioned transgenic models of PA are associated with the onset of autonomous aldosterone production at birth. Thus, these models do not accurately recapitulate PA, as it is typically an adult-onset disease. Furthermore, the aldosterone excess in these mouse models is not reversible. Mice can also be treated with mineralocorticoids to study the peripheral effects of mineralocorticoid receptor activation, however these models do not include the diseased adrenal component that causes PA. In addition, the minipumps used for administration of aldosterone, as well as the cost of this steroid, limit this experimental approach. Therefore, the *AS*$^{+/Cre}$ *hM3Dq* mouse model provides an attractive transgenic PA model that is inducible and reversible and, to our knowledge, represents the first use of DREADD technology in the adrenal gland.

Future studies will be needed to determine the cause of the sexual dimorphism observed in the *AS*$^{+/Cre}$ *hM3Dq* mouse line. This dimorphism can partially be attributed to a slower rate of adrenocortical cell turnover in male mice compared with female mice, resulting in lower levels of the hM3Dq receptor in males until late in life (49, 85). Also, a recent study reported sex differences in the mechanism of cell renewal within the adrenal cortex that appears to be influenced by adrenal androgens (85). However, the rather large disparity between male and female responses implies that additional underlying factors may be at play. Sexual dimorphism in the mouse adrenal gland is well established, with clear sex differences in gene expression observed within the adrenal gland (86). Several previous mouse models of adrenal dysfunction have had varying results between the sexes (49, 67, 68, 70, 75, 87). This further argues for a sex-dependent mechanism of adrenal regulation, possibly driven by androgens or estrogens.

In summary, this study supports a role for Gq signaling in adrenocortical functional zonation and the induction of an aldosterone-producing cell phenotype. Our findings indicate that the Gq signaling pathway is sufficient to trigger Cyp11b2 expression in non-aldosterone-producing ZF cells. This observation suggests that adrenocortical cells possess plasticity in their steroidogenic potential, whereby their steroidogenic function can be transformed with activation of the appropriate signaling cascade. Nevertheless, further work will be needed to address whether Gq signaling is necessary for physiologic maintenance of a ZG cellular identity. Future studies using the *AS*$^{+/Cre}$ *hM3Dq* mouse line will also aid in defining the mechanisms whereby sustained inappropriate aldosterone production causes deleterious effects in peripheral tissues and provide a preclinical model for investigating potential PA therapeutic targets.

Methods

Mice. Both the *AS*-Cre (1) and *hM3Dq* (47) mouse lines have been previously described. *AS*$^{+/Cre}$ *hM3Dq* mice were maintained on a mixed background, with littermate controls used when possible to control for genetic variability. Mice in all experiments were 18–22 weeks of age at the start of each experimental protocol. CNO (Tocris Bioscience) was dissolved in DMSO at 30 mg/mL. CNO-treated mice were

administered 50 μg/mL CNO in the drinking water in addition to 5 mM saccharin for taste. Vehicle-treated mice were administered 5 mM saccharin and 0.17% DMSO (as with the CNO-treated mice). Drinking water was provided ad libitum and replaced every 2 days. Mice were fed a standard chow diet ad libitum (Research Diets) or a HS diet (Envigo) that contained 4% NaCl. All mice were maintained on a 12-hour light/12-hour dark cycle. Mice were housed in the Unit for Laboratory Animal Management at the University of Michigan. Mice were sacrificed using the decapitation method to ensure that there was minimal effect on the hypothalamic/pituitary/adrenal axis.

qPCR analysis. RNA was isolated from whole adrenal glands using the bead homogenization method and the RNeasy Plus Mini Kit (QIAGEN). In kidney experiments, frozen kidneys were first pulverized into a frozen powder that was used for RNA extraction. Reverse transcription was performed using the High Capacity cDNA Reverse Transcription Kit (Applied Biosystems). qPCR was performed using TaqMan or SYBR green primer sets, and data were analyzed according to relative expression using the ΔΔCt method. *Ppia* was used as the housekeeping gene for analysis. The TaqMan primers from Applied Biosystems were as follows: *Cyp11a1* (Mm00490735_m1); *Cyp21a1* (Mm00487230_g1); *Hsd3b1* (Mm01261921_mH); *Ppia* (Rn00690933_m1); *Ren1* (Mm02342887_mH); and *Star* (Mm00441558_m1). The TaqMan primers designed by Integrated DNA Technologies were as follows: *Cyp11b1* F (5′-GTCCTCAATGTGAATCTGTATTCCA-3′); *Cyp11b1* R (5′-CCAGCGCTGAGGCATATAGC-3′); *Cyp11b1* probe (5′-56-FAM/CCGGAACCCTGCAGTG-3′); *Cyp11b2* forward (5′-TGCTGGGACATTGGTCCTACT-3′); *Cyp11b2* reverse (5′-CTTGGGAACACTGCAGGGTT-3′); and *Cyp11b2* probe (5′-56-FAM/TATCTCTAC/ZEN/TCCATGGGC-3′). The SYBR green primer sets from Integrated DNA Technologies were as follows: *Axin2* F (5′-GAGGATGCTGAAGGCTCAAA-3′); *Axin2* R (5′-GCAGGCAAATTCGTCACTC-3′); *Dab2* forward (5′-TGTTGGCCAGGTTCAAAGGT-3′); and *Dab2* reverse (5′-GCACATCATCAATACCGATTAGCT-3′).

IF and histology. Whole adrenal glands were fixed in 4% paraformaldehyde for 1 hour. These tissues were processed, embedded in paraffin, and sectioned at 5-μm thickness. For IF analysis, antigen retrieval was performed followed by 1 hour of blocking for nonspecific staining. Blocking reagents included 5% normal goat serum (NGS) in PBS (HA tag), 10% NGS with 0.5% SDS in PBS containing Tween-20 (Cyp11b1/Cyp11b2), 2.5% normal horse serum (NHS) with 1% BSA in PBS (β-catenin), or 2.5% NHS with the M.O.M. Kit (Vector Laboratories) in PBS (Dab2). Primary antibodies were incubated overnight at 4°C. The antibodies used were anti-HA High Affinity (1:500, Roche, 11867423001); anti-Cyp11b2 (1:200, provided by C. Gomez-Sanchez, University of Mississippi); anti-Cyp11b1 (1:100, provided by C. Gomez-Sanchez, University of Mississippi); anti-Dab2 (1:500, BD Biosciences, no. 610464); and anti–β-catenin (1:500, Cell Signaling Technology, no. 8814). IF detection was accomplished using Alexa Fluor–conjugated secondary antibodies (from Jackson ImmunoResearch and Thermo Fisher Scientific) or HRP-polymer solution (Vector Laboratories) and Alexa Fluor tyramide reagent (Thermo Fisher Scientific). Histologic analysis of tissues was assessed on H&E-stained sections. Sections processed for IF and H&E staining were imaged using an Axio Imager M2 (Zeiss).

Steroid measurements. Trunk blood from decapitated mice was collected in sodium heparin tubes, and plasma was isolated by centrifugation. We quantified four C_{18} steroids (11-deoxycorticosterone, corticosterone, 18OHB, and aldosterone) using liquid chromatography–tandem mass spectrometry (LC-MS/MS). Unlabeled and deuterium-labeled steroids were obtained from Sigma-Aldrich, Cerilliant, and C/D/N Isotopes (Supplemental Table 2). Steroid extraction by liquid-liquid extraction and quantitation were performed as previously described (88).

Samples (10-μL) were injected via autosampler and resolved with a pair of Agilent 1260/1290 binary pump HPLCs via 2D liquid chromatography, first on a 10 × 3 mm, 3-μm particle size Hypersil Gold C4 loading column (Thermo Fisher Scientific) followed by a Kinetex 50 × 2.1 mm, 2.6-μm particle size biphenyl resolving column (Phenomenex). The mobile phases consisted of 0.2 mmol/L aqueous ammonium fluoride (mobile phase A) and methanol with 0.2 mmol/L ammonium fluoride (mobile phase B). Steroids were eluted using gradient specifications as described in Supplemental Table 3. The column effluent was directed into the source of an Agilent 6495 triple quadrupole mass spectrometer using electrospray ionization in positive ion mode for Δ4 and analyzed using multiple reaction monitoring (MRM) mode (Supplemental Table 3). Quantitation was performed by comparing ion currents for the monitored ions with weighted (1/×) 12-point linear external calibration curves (r2 was >0.995) and corrected for specimen dilution and recovery of internal standards using ChemStation and MassHunter software (Agilent Technologies). Intra-assay and inter-assay coefficients of variation (CV) were assessed by measuring quality control–pooled serum samples 5 times within a run and across 5 different runs, respectively, and they were less than 12% for all steroids. The lower limit of detection (LOD) for each steroid was defined by the minimum concentration achieving an extrapolated signal-to-noise ratio of 3, and it ranged from 3.0 pg/mL for aldosterone to 44.4 pg/mL for corticosterone (Supplemental Table 2).

Plasma renin. Mouse plasma renin was measured by an ELISA specific for the detection of Mouse Renin 1 (Thermo Fisher Scientific). Plasma samples were diluted 15-fold in the kit-provided diluent A and run in duplicate.

Radiotelemetry. Mice were surgically implanted with a telemetric blood pressure transducer (Data Sciences International [DSI]) by the University of Michigan Physiology Phenotyping Core as previously described (89). The catheter of the device was passed into the carotid artery, and the transducer was placed in the abdominal cavity. Mice were monitored postoperatively and given 2 weeks to recover from surgery prior to treatment. Mice were individually housed in cages atop receiver pads, allowing for real-time measurements of blood pressure. As stated by DSI, the mean pressure parameter value was calculated by averaging the pressure values over 50 subsegments of the segment length. For our 24-hour analysis (Figure 6C), we selected the final day of the HS diet alone, the second day of the HS plus CNO treatment (near the peak MAP in most mice), and the seventh day of the washout period (when MAP returned closest to baseline and stabilized in most mice).

Statistics. Data are presented as the mean ± SEM. The box-and-whisker plots in Figure 6B depict the interquartile range between the 25th and 75th percentiles and the median (box), along with the maximum and minimum values (whiskers). An unpaired, 2-tailed Student's *t* test was used for comparisons of groups of 2. A 1-way ANOVA with Bonferroni's post hoc test was used for groups of 3 or more. For Figure 6B, a repeated-measures 1-way ANOVA with Bonferroni's correction for multiple comparisons was performed. Comparisons of hourly blood pressure values (Figure 6C) were made using a repeated-measures 2-way ANOVA with Bonferroni's correction. All immunofluorescence experiments were performed using 5 or more mice. Statistical

tests were calculated using GraphPad Prism 7.0 (GraphPad Software). A *P* value of less than 0.05 was considered statistically significant.

Study approval. All mouse procedures were approved by the IACUC of the University of Michigan.

Author contributions

MJT and WER designed the study. MJT, MRU, ECF, and JR performed experiments and acquired the data. EL and SB provided early conceptual design and preliminary experimental data using a *Cyp11a1*-Cre adrenal DREADD mouse line. MJT and WER analyzed the data. MSA characterized the *hM3Dq* allele. EL, MSA, and DTB provided the mouse lines and consultation on their use. CEGS provided antibodies and consultation on immunofluorescence protocols. MJT and WER wrote the manuscript. WER supervised the study.

Acknowledgments

This project was supported by grants from the NIH (DK043140, to WER and GM008322, to MJT) and the American Heart Association (AHA) (16PRE29620010, to MJT). We thank Anne Teissier from the French National Center for Scientific Research for her work characterizing the *hM3Dq* allele and mouse line. We also thank Steven E. Whitesall and Daniel E. Michele from the University of Michigan Phenotyping Core for their collaboration on the radiotelemetry surgeries, experiments, and data analysis.

Address correspondence to: William E. Rainey, Department of Molecular and Integrative Physiology, University of Michigan, 1150 West Medical Center Drive, 2560C Medical Science Research Building II, Ann Arbor, Michigan 48109-5622, USA. Phone: 734.764.7514; Email: wer@umich.edu.

1. Freedman BD, et al. Adrenocortical zonation results from lineage conversion of differentiated zona glomerulosa cells. *Dev Cell*. 2013;26(6):666–673.
2. Chang SP, Morrison HD, Nilsson F, Kenyon CJ, West JD, Morley SD. Cell proliferation, movement and differentiation during maintenance of the adult mouse adrenal cortex. *PLoS ONE*. 2013;8(12):e81865.
3. Iannaccone P, Morley S, Skimina T, Mullins J, Landini G. Cord-like mosaic patches in the adrenal cortex are fractal: implications for growth and development. *FASEB J*. 2003;17(1):41–43.
4. Morley SD, Viard I, Chung BC, Ikeda Y, Parker KL, Mullins JJ. Variegated expression of a mouse steroid 21-hydroxylase/beta- galactosidase transgene suggests centripetal migration of adrenocortical cells. *Mol Endocrinol*. 1996;10(5):585–598.
5. McNicol AM, Duffy AE. A study of cell migration in the adrenal cortex of the rat using bromodeoxyuridine. *Cell Tissue Kinet*. 1987;20(5):519–526.
6. Zajicek G, Ariel I, Arber N. The streaming adrenal cortex: direct evidence of centripetal migration of adrenocytes by estimation of cell turnover rate. *J Endocrinol*. 1986;111(3):477–482.
7. Bertholet JY. Proliferative activity and cell migration in the adrenal cortex of fetal and neonatal rats: an autoradiographic study. *J Endocrinol*. 1980;87(1):1–9.
8. Pignatti E, Leng S, Carlone DL, Breault DT. Regulation of zonation and homeostasis in the adrenal cortex. *Mol Cell Endocrinol*. 2017;441:146–155.
9. Kataoka Y, Ikehara Y, Hattori T. Cell proliferation and renewal of mouse adrenal cortex. *J Anat*. 1996;188(Pt 2):375–381.
10. Fern RJ, Hahm MS, Lu HK, Liu LP, Gorelick FS, Barrett PQ. Ca2+/calmodulin-dependent protein kinase II activation and regulation of adrenal glomerulosa Ca2+ signaling. *Am J Physiol*. 1995;269(6 Pt 2):F751–F760.
11. Ganguly A, Davis JS. Role of calcium and other mediators in aldosterone secretion from the adrenal glomerulosa cells. *Pharmacol Rev*. 1994;46(4):417–447.
12. Bird IM, et al. Human NCI-H295 adrenocortical carcinoma cells: a model for angiotensin-II-responsive aldosterone secretion. *Endocrinology*. 1993;133(4):1555–1561.
13. Bollag WB, Barrett PQ, Isales CM, Rasmussen H. Angiotensin-II-induced changes in diacylglycerol levels and their potential role in modulating the steroidogenic response. *Endocrinology*. 1991;128(1):231–241.
14. Hunyady L, Baukal AJ, Bor M, Ely JA, Catt KJ. Regulation of 1,2-diacylglycerol production by angiotensin-II in bovine adrenal glomerulosa cells. *Endocrinology*. 1990;126(2):1001–1008.
15. Barrett PQ, Bollag WB, Isales CM, McCarthy RT, Rasmussen H. Role of calcium in angiotensin II-mediated aldosterone secretion. *Endocr Rev*. 1989;10(4):496–518.
16. Kojima I, Kojima K, Kreutter D, Rasmussen H. The temporal integration of the aldosterone secretory response to angiotensin occurs via two intracellular pathways. *J Biol Chem*. 1984;259(23):14448–14457.
17. Farese RV, Larson RE, Sabir MA, Gomez-Sanchez C. Effects of angiotensin-II and potassium on phospholipid metabolism in the adrenal zona glomerulosa. *J Biol Chem*. 1981;256(21):11093–11097.
18. Bassett MH, Suzuki T, Sasano H, White PC, Rainey WE. The orphan nuclear receptors NURR1 and NGFIB regulate adrenal aldosterone production. *Mol Endocrinol*. 2004;18(2):279–290.
19. Breault L, Lehoux JG, Gallo-Payet N. Angiotensin II receptors in the human adrenal gland. *Endocr Res*. 1996;22(4):355–361.
20. Monticone S, et al. Prevalence and clinical manifestations of primary aldosteronism encountered in primary care practice. *J Am Coll Cardiol*. 2017;69(14):1811–1820.
21. Hannemann A, Wallaschofski H. Prevalence of primary aldosteronism in patient's cohorts and in population-based studies--a review of the current literature. *Horm Metab Res*. 2012;44(3):157–162.
22. Rossi GP, et al. A prospective study of the prevalence of primary aldosteronism in 1,125 hypertensive patients. *J Am Coll Cardiol*. 2006;48(11):2293–2300.
23. Strauch B, Zelinka T, Hampf M, Bernhardt R, Widimsky J Jr. Prevalence of primary hyperaldosteronism in moderate to severe hypertension in the Central Europe region. *J Hum Hypertens*. 2003;17(5):349–352.
24. Calhoun DA, Nishizaka MK, Zaman MA, Thakkar RB, Weissmann P. Hyperaldosteronism among black and white subjects with resistant hypertension. *Hypertension*. 2002;40(6):892–896.
25. Lim PO, Dow E, Brennan G, Jung RT, MacDonald TM. High prevalence of primary aldosteronism in the Tayside hypertension clinic population. *J Hum Hypertens*. 2000;14(5):311–315.
26. Fardella CE, et al. Primary hyperaldosteronism in essential hypertensives: prevalence, biochemical profile, and molecular biology. *J Clin Endocrinol Metab*. 2000;85(5):1863–1867.
27. Savard S, Amar L, Plouin PF, Steichen O. Cardiovascular complications associated with primary aldosteronism: a controlled cross-sectional study. *Hypertension*. 2013;62(2):331–336.
28. Mulatero P, et al. Long-term cardio- and cerebrovascular events in patients with primary aldosteronism. *J Clin Endocrinol Metab*. 2013;98(12):4826–4833.
29. Catena C, et al. Cardiovascular outcomes in patients with primary aldosteronism after treatment. *Arch Intern Med*. 2008;168(1):80–85.
30. Milliez P, Girerd X, Plouin PF, Blacher J, Safar ME, Mourad JJ. Evidence for an increased rate of cardiovascular events in patients with primary aldosteronism. *J Am Coll Cardiol*. 2005;45(8):1243–1248.
31. Gekle M, Grossmann C. Actions of aldosterone in the cardiovascular system: the good, the bad, and the ugly? *Pflugers Arch*. 2009;458(2):231–246.
32. Hayashi H, et al. Aldosterone nongenomically produces NADPH oxidase-dependent reactive oxygen species and induces myocyte apoptosis. *Hypertens Res*. 2008;31(2):363–375.
33. Tsybouleva N, et al. Aldosterone, through novel signaling proteins, is a fundamental molecular bridge between the genetic defect and the cardiac phenotype of hypertrophic cardiomyopathy. *Circulation*. 2004;109(10):1284–1291.
34. Qin W, et al. Transgenic model of aldosterone-driven cardiac hypertrophy and heart failure. *Circ Res*. 2003;93(1):69–76.
35. Lijnen P, Petrov V. Induction of cardiac fibrosis by aldosterone. *J Mol Cell Cardiol*. 2000;32(6):865–879.
36. Aragao-Santiago L, Gomez-Sanchez CE, Mulatero P, Spyroglou A, Reincke M, Williams TA. Mouse models of primary aldosteronism: from physiology to pathophysiology. *Endocrinology*. 2017;158(12):4129–4138.
37. Urban DJ, Roth BL. DREADDs (designer recep-

tors exclusively activated by designer drugs): chemogenetic tools with therapeutic utility. *Annu Rev Pharmacol Toxicol*. 2015;55:399–417.
38. Armbruster BN, Li X, Pausch MH, Herlitze S, Roth BL. Evolving the lock to fit the key to create a family of G protein-coupled receptors potently activated by an inert ligand. *Proc Natl Acad Sci USA*. 2007;104(12):5163–5168.
39. Vardy E, et al. A new DREADD facilitates the multiplexed chemogenetic interrogation of behavior. *Neuron*. 2015;86(4):936–946.
40. Agulhon C, Boyt KM, Xie AX, Friocourt F, Roth BL, McCarthy KD. Modulation of the autonomic nervous system and behaviour by acute glial cell Gq protein-coupled receptor activation in vivo. *J Physiol (Lond)*. 2013;591(22):5599–5609.
41. Li JH, et al. A novel experimental strategy to assess the metabolic effects of selective activation of a G(q)-coupled receptor in hepatocytes in vivo. *Endocrinology*. 2013;154(10):3539–3551.
42. Yagi H, et al. A synthetic biology approach reveals a CXCR4-G13-Rho signaling axis driving transendothelial migration of metastatic breast cancer cells. *Sci Signal*. 2011;4(191):ra60.
43. Vaqué JP, et al. A genome-wide RNAi screen reveals a Trio-regulated Rho GTPase circuitry transducing mitogenic signals initiated by G protein-coupled receptors. *Mol Cell*. 2013;49(1):94–108.
44. Dell'Anno MT, et al. Remote control of induced dopaminergic neurons in parkinsonian rats. *J Clin Invest*. 2014;124(7):3215–3229.
45. Guettier JM, et al. A chemical-genetic approach to study G protein regulation of beta cell function in vivo. *Proc Natl Acad Sci USA*. 2009;106(45):19197–19202.
46. Jain S, Ruiz de Azua I, Lu H, White MF, Guettier JM, Wess J. Chronic activation of a designer G(q)-coupled receptor improves β cell function. *J Clin Invest*. 2013;123(4):1750–1762.
47. Teissier A, et al. Activity of Raphé serotonergic neurons controls emotional behaviors. *Cell Rep*. 2015;13(9):1965–1976.
48. Alexander GM, et al. Remote control of neuronal activity in transgenic mice expressing evolved G protein-coupled receptors. *Neuron*. 2009;63(1):27–39.
49. Dumontet T, et al. PKA signaling drives reticularis differentiation and sexually dimorphic adrenal cortex renewal. *JCI Insight*. 2018;3(2):98394.
50. Engeland WC, et al. The adrenal clock prevents aberrant light-induced alterations in circadian glucocorticoid rhythms. *Endocrinology*. 2018;159(12):3950–3964.
51. Romero DG, et al. Disabled-2 is expressed in adrenal zona glomerulosa and is involved in aldosterone secretion. *Endocrinology*. 2007;148(6):2644–2652.
52. Walczak EM, et al. Wnt signaling inhibits adrenal steroidogenesis by cell-autonomous and non-cell-autonomous mechanisms. *Mol Endocrinol*. 2014;28(9):1471–1486.
53. Berthon A, et al. Constitutive beta-catenin activation induces adrenal hyperplasia and promotes adrenal cancer development. *Hum Mol Genet*. 2010;19(8):1561–1576.
54. Kim AC, et al. Targeted disruption of beta-catenin in Sf1-expressing cells impairs development and maintenance of the adrenal cortex. *Development*. 2008;135(15):2593–2602.
55. Drelon C, et al. PKA inhibits WNT signalling in adrenal cortex zonation and prevents malignant tumour development. *Nat Commun*. 2016;7:12751.
56. Finco I, Lerario AM, Hammer GD. Sonic hedgehog and WNT signaling promote adrenal gland regeneration in male mice. *Endocrinology*. 2018;159(2):579–596.
57. Berthon A, et al. WNT/beta-catenin signalling is activated in aldosterone-producing adenomas and controls aldosterone production. *Hum Mol Genet*. 2014;23(4):889–905.
58. Basham KJ, et al. A ZNRF3-dependent Wnt/β-catenin signaling gradient is required for adrenal homeostasis. *Genes Dev*. 2019;33(3-4):209–220.
59. Holland OB, Carr B. Modulation of aldosterone synthase messenger ribonucleic acid levels by dietary sodium and potassium and by adrenocorticotropin. *Endocrinology*. 1993;132(6):2666–2673.
60. Scortegagna M, et al. The E3 ubiquitin ligase Siah1 regulates adrenal gland organization and aldosterone secretion. *JCI Insight*. 2017;2(23):97128.
61. Peng KY, et al. miRNA-203 modulates aldosterone levels and cell proliferation by targeting Wnt5a in aldosterone-producing adenomas. *J Clin Endocrinol Metab*. 2018;103(10):3737–3747.
62. Wu VC, et al. The prevalence of CTNNB1 mutations in primary aldosteronism and consequences for clinical outcomes. *Sci Rep*. 2017;7:39121.
63. Åkerström T, et al. Activating mutations in CTNNB1 in aldosterone producing adenomas. *Sci Rep*. 2016;6:19546.
64. Tadjine M, Lampron A, Ouadi L, Bourdeau I. Frequent mutations of beta-catenin gene in sporadic secreting adrenocortical adenomas. *Clin Endocrinol (Oxf)*. 2008;68(2):264–270.
65. Tissier F, et al. Mutations of beta-catenin in adrenocortical tumors: activation of the Wnt signaling pathway is a frequent event in both benign and malignant adrenocortical tumors. *Cancer Res*. 2005;65(17):7622–7627.
66. Bandulik S, Penton D, Barhanin J, Warth R. TASK1 and TASK3 potassium channels: determinants of aldosterone secretion and adrenocortical zonation. *Horm Metab Res*. 2010;42(6):450–457.
67. Heitzmann D, et al. Invalidation of TASK1 potassium channels disrupts adrenal gland zonation and mineralocorticoid homeostasis. *EMBO J*. 2008;27(1):179–187.
68. Davies LA, et al. TASK channel deletion in mice causes primary hyperaldosteronism. *Proc Natl Acad Sci USA*. 2008;105(6):2203–2208.
69. El Wakil A, et al. Dkk3 is a component of the genetic circuitry regulating aldosterone biosynthesis in the adrenal cortex. *Hum Mol Genet*. 2012;21(22):4922–4929.
70. Penton D, et al. Task3 potassium channel gene invalidation causes low renin and salt-sensitive arterial hypertension. *Endocrinology*. 2012;153(10):4740–4748.
71. Guagliardo NA, et al. TASK-3 channel deletion in mice recapitulates low-renin essential hypertension. *Hypertension*. 2012;59(5):999–1005.
72. Grimm PR, Irsik DL, Settles DC, Holtzclaw JD, Sansom SC. Hypertension of Kcnmb1-/- is linked to deficient K secretion and aldosteronism. *Proc Natl Acad Sci USA*. 2009;106(28):11800–11805.
73. Sausbier M, et al. Elevated blood pressure linked to primary hyperaldosteronism and impaired vasodilation in BK channel-deficient mice. *Circulation*. 2005;112(1):60–68.
74. Doi M, et al. Salt-sensitive hypertension in circadian clock-deficient Cry-null mice involves dysregulated adrenal Hsd3b6. *Nat Med*. 2010;16(1):67–74.
75. Spyroglou A, et al. Utilization of a mutagenesis screen to generate mouse models of hyperaldosteronism. *Endocrinology*. 2011;152(1):326–331.
76. Makhanova N, Hagaman J, Kim HS, Smithies O. Salt-sensitive blood pressure in mice with increased expression of aldosterone synthase. *Hypertension*. 2008;51(1):134–140.
77. Gu H, et al. Salt-dependent blood pressure in human aldosterone synthase-transgenic mice. *Sci Rep*. 2017;7(1):492.
78. Huang CC, Miyagawa S, Matsumaru D, Parker KL, Yao HH. Progenitor cell expansion and organ size of mouse adrenal is regulated by sonic hedgehog. *Endocrinology*. 2010;151(3):1119–1128.
79. Billet S, Bardin S, Tacine R, Clauser E, Conchon S. The AT1A receptor "gain-of-function" mutant N111S/delta329 is both constitutively active and hyperreactive to angiotensin II. *Am J Physiol Endocrinol Metab*. 2006;290(5):E840–E848.
80. St-Jean M, Ghorayeb NE, Bourdeau I, Lacroix A. Aberrant G-protein coupled hormone receptor in adrenal diseases. *Best Pract Res Clin Endocrinol Metab*. 2018;32(2):165–187.
81. Saner-Amigh K, et al. Elevated expression of luteinizing hormone receptor in aldosterone-producing adenomas. *J Clin Endocrinol Metab*. 2006;91(3):1136–1142.
82. Lampron A, et al. Regulation of aldosterone secretion by several aberrant receptors including for glucose-dependent insulinotropic peptide in a patient with an aldosteronoma. *J Clin Endocrinol Metab*. 2009;94(3):750–756.
83. Zwermann O, Suttmann Y, Bidlingmaier M, Beuschlein F, Reincke M. Screening for membrane hormone receptor expression in primary aldosteronism. *Eur J Endocrinol*. 2009;160(3):443–451.
84. Teo AE, et al. Pregnancy, primary aldosteronism, and adrenal CTNNB1 mutations. *N Engl J Med*. 2015;373(15):1429–1436.
85. Grabek A, Dolfi B, Klein B, Jian-Motamedi F, Chaboissier MC, Schedl A. The adult adrenal cortex undergoes rapid tissue renewal in a sex-specific manner. *Cell Stem Cell*. 2019;25(2):290–296.e2.
86. El Wakil A, Mari B, Barhanin J, Lalli E. Genomic analysis of sexual dimorphism of gene expression in the mouse adrenal gland. *Horm Metab Res*. 2013;45(12):870–873.
87. Spyroglou A, et al. Diastrophic dysplasia sulfate transporter (SLC26A2) is expressed in the adrenal cortex and regulates aldosterone secretion. *Hypertension*. 2014;63(5):1102–1109.
88. Guasti L, Paul A, Laufer E, King P. Localization of Sonic hedgehog secreting and receiving cells in the developing and adult rat adrenal cortex. *Mol Cell Endocrinol*. 2011;336(1-2):117–122.
89. Whitesall SE, Hoff JB, Vollmer AP, D'Alecy LG. Comparison of simultaneous measurement of mouse systolic arterial blood pressure by radiotelemetry and tail-cuff methods. *Am J Physiol Heart Circ Physiol*. 2004;286(6):H2408–H2415.